Inorganica Chimica Acta 549 (2023) 121403

Contents lists available at ScienceDirect

Inorganica Chimica Acta

journal homepage: www.elsevier.com/locate/ica

Research paper

Crystal structures, antioxidant, electrochemical and *in-situ* spectroelectrochemical properties of new bisthiocarbohydrazones and their Ni(II) complexes

Yeliz Kaya [a], Ayşe Erçağ [a,*], Özlem Uğuz [b], Yunus Zorlu [c], Atıf Koca [b]

[a] Istanbul University-Cerrahpaşa, Faculty of Engineering, Department of Chemistry, Inorganic Chemistry Division, Avcılar, Istanbul 34320, Turkey
[b] Engineering Faculty, Chemical Engineering Department, Marmara University, Istanbul, Turkey
[c] Gebze Technical University, Department of Chemistry, Gebze, Kocaeli 41400, Turkey

ARTICLE INFO

Keywords:
Electrochemistry
Bisthiocarbohydrazone
Nickel(II)
Crystal structure
Antioxidant

ABSTRACT

Four new isatin bisthiocarbohydrazone ligands (H_2L1, H_2L2, H_2L3, H_2L4) were synthesized by the condensation of salicylaldehyde, 5-bromosalicylaldehyde, 5-chlorosalicylaldehyde and 5-nitrosalicylaldehyde with isatin monothiocarbohydrazone, respectively. The mixed ligand Ni(II) complexes {[NiL1(P)], [NiL2(P)], [NiL3(P)] and [NiL4(P)]} containing triphenylphosphine (P: triphenylphosphine, PPh_3) of these bisthiocarbohydrazone ligands were synthesized. The synthesized compounds were characterized by elemental analysis, FT-IR, ^{1}H NMR, UV–Vis spectroscopy techniques and conductivity measurements. In the complexes, the bisthiocarbohydrazone ligands coordinate to nickel through ONS mode. The complexes are diamagnetic and exhibit square planar geometry. The crystal structures of two ligands, H_2L1 and H_2L3, and two complexes, [NiL1(P)] and $[Ni_3(L3)_2(P)_2]$, whose single crystals were obtained, were determined by single crystal X-ray diffraction technique. The crystal structure of [NiL1(P)] complex is monomeric and compatible with the structure of the solid complex. A new trinuclear Ni(II) complex, $[Ni_3(L3)_2(P)_2]$, was obtained by the crystallization of monomeric solid [NiL3(P)] complex in a different solvent mixture. Redox properties of bisthiocarbohydrazone ligands (H_2L1-H_2L4) bearing S1 or S2 substituents and their nickel(II) complexes {[NiL1(P)]-[NiL4(P)]} were investigated with cyclic voltammetry and *in situ* spectroelectrochemistry. Voltammetric analyses indicated that all ligands exhibited four quasi-reversible reduction and one irreversible oxidation process. Complexation of the ligands with Ni(II) cation decreased the number of the reduction processes and caused these processes to have more negative potentials. Significant spectral changes were also observed in the *in situ* spectroelectrochemical analysis due to electron transfer reactions. In addition, electrochemical responses of monosubstituted salicylaldehyde derivative isatin bisthiocarbohydrazone ligands and their nickel(II) complexes were compared with their disubstituted derivatives.

1. Introduction

Thiocarbohydrazones may contain one or two azomethine (-C═N-) bonds that can link one or more aromatic/heterocyclic rings to form different molecular structures [1]. Monothiocarbohydrazone compounds are obtained by the imminating of a hydrazine group, and bisthiocarbohydrazone compounds are obtained by the reaction of two hydrazine groups [2,3]. If both carbonyl compounds added to the thiocarbohydrazide are the same, symmetrical bisthiocarbohydrazones are formed, and if they are different, asymmetrical bisthiocarbohydrazones are formed [2,3].

Sulfur atom and imine nitrogen are active groups for complexation in thiocarbohydrazone compounds [4]. Moreover, tridentate or tetradentate thiocarbohydrazones can be obtained by the presence of additional coordination sites from aldehyde or ketone [2–4].

The structure-activity relationships (SAR) revealed that halogen (F, Cl and Br) and nitro (NO_2) substituents on the benzylidene moiety lead to the most active compounds. The presence of these substituents has been shown to increase antifungal activity [5].

It is known that isatin compounds have a wide variety of pharmacological properties, including antibacterial, anticonvulsant, anti-HIV and antifungal activity [6–9].

It has been disclosed that thiocarbohydrazone compounds containing isatin exhibit various chemotherapeutic activities and can be used as

* Corresponding author.
E-mail address: ercaga@iuc.edu.tr (A. Erçağ).

https://doi.org/10.1016/j.ica.2023.121403
Received 21 November 2022; Received in revised form 18 January 2023; Accepted 20 January 2023
Available online 23 January 2023

synthetic antioxidants to suppress cell damage against reactive oxygen species [10–12].

Nickel is a trace element found in human, animal and plant metabolism [13,14]. It has been reported that many enzymes contain nickel in their structure [15]. Antiviral, antioxidant, antifungal, anticarcinogenic, antibacterial and antitumor activities of phosphine-based ligands and complexes containing this molecule were tested. These complexes can play vital roles in controlling gene expression and inhibiting cell division [16,17].

In our previous study, we reported the synthesis, characterization, and some properties of bisthiocarbohydrazone ligands derived from isatin monothiocarbohydrazone with halogen disubstituted salicylaldehydes and their Ni(II) complexes [18].

In this study, we planned to prepare new bisthiocarbohydrazone compounds and their Ni(II) complexes derived from isatin monothiocarbohydrazone and halogen monosubstituted salicylaldehydes in order to detail their structures and some properties and to compare them with the previous ones.

Four new asymmetric isatin bisthiocarbohydrazone ligands (H_2L1, H_2L2, H_2L3 and H_2L4) were synthesized using isatin monothiocarbohydrazone and related aldehydes (salicylaldehyde, 5-bromosalicylaldehyde, 5-chlorosalicylaldehyde and 5-nitrosalicylaldehyde, respectively). Four new solid Ni(II) complexes {[NiL1(P)]-[NiL4(P)]} were isolated from the reaction of these ligands with Ni(II) ions in the presence of triphenylphosphine. The synthesized compounds were characterized by a combination of elemental analysis, IR, ^{1}H NMR and UV–Vis. These compounds have not been previously reported in the literature. In single crystal extraction studies, single crystals of two ligands (H_2L1 and H_2L3) and two complexes {[NiL1(P)] and $[Ni_3(L3)_2(P)_2]$} were obtained and their crystal structures were elucidated by X-ray diffraction method. The crystal structure of the [NiL1(P)] complex is monomeric and compatible with the structure of the solid complex. A new trinuclear Ni(II) complex, $[Ni_3(L3)_2(P)_2]$, was obtained by crystallization of monomeric solid [NiL3(P)] complex in a different solvent mixture.

In the literature, there are some articles on the application of isatin hydrazone ligands and metal complexes as corrosion inhibitors, and their use in energy conversion and storage devices [19–21], for instance, Oliveira-Brett et al. [22] reported a detailed electrochemical study of isatin nitro-derivatives showing two ligand-based reduction and one ligand-based oxidation reactions [22]. The same authors also published the electrochemical behavior of a series of isatin derivatives. There are also some surface electrochemical studies on various copper(II) complexes of isatin derivatives [23,24]. However, studies on detailed electrochemical and especially spectroelectrochemical analyzes of isatin thiocarbohydrazone compounds are very few. As we mentioned in our previous publication, these studies are quite new for asymmetric isatin bisthiocarbohydrazone compounds [18]. In that article, we reported that while the free isatin thiocarbohydrazone ligands illustrated one oxidation and four reduction waves, the Ni(II) complexes gave an additional metal based oxidation, which considerably influenced the in-situ spectroelectrochemical responses of the ligands. In our previous papers, we have reported electrochemical responses of similar thiosemicarbazone ligands and their complexes and we observed that the ligand type considerably influenced the redox activities, and the redox activities are the key factor for their possible applications [25–29].

Here, comprehensive redox activity of monosubstituted salicylaldehyde-derived asymmetric isatin bisthiocarbohydrazone ligands and their mixed ligand nickel(II) complexes were investigated to compare with their disubstituted derivatives [18] and to give an idea about their application areas.

2. Experimental section

2.1. Materials and instrumentation

Thiocarbohydrazide was synthesized according to the literature procedure [30]. All other chemicals and solvents were of commercial reagent grade and used as received from Aldrich, Merck and Alfa Aesar.

Elemental analyses (C, H, N and S) were carried out on a Thermo Finnigan Flash EA 1112 Series Elemental Analyzer. UV–Vis spectra were recorded in DMF solutions on the Shimadzu 2600 UV–Vis Spectrophotometer. Infrared spectra were recorded by using an Agilent Cary 630 FTIR-ATR spectrometer. ^{1}H NMR spectra were determined by a Varian UNITY INOVA 500 MHz NMR spectrometer using DMSO-d_6 as solvent at 25 ± 2 °C. Antioxidant properties of synthesized compounds were performed by a Shimadzu 2600 UV–vis spectrophotometer. Magnetic measurements were carried out using the Gouy technique with the MK I model device obtained from Sherwood Scientific at room temperature. Molar conductivities of the complexes were measured on a digital WPA CMD 750 conductivity meter in DMSO (10^{-3} M) at 25 ± 2 °C.

2.2. Synthesis of the ligands

2.2.1. Synthesis of 1-(2-oxoindolin-3-ylidene)thiocarbohydrazone, L

1-(2-oxoindolin-3-ylidene)thiocarbohydrazone (L) was prepared as described in the literature [18,31].

2.2.2. Synthesis of 1-[2-oxoindolin-3-ylidene]-5-[2-hydroxyphenyl)methylidene]thiocarbohydrazone, H_2L1

1 mmol of salicylaldehyde in ethanol (10 mL) was added to a solution of 1-(2-oxoindolin-3-ylidene)thiocarbohydrazone (L) (1 mmol) in ethanol (15 mL) and DMF (5 mL). The resulting mixture was refluxed for 4 h, formation of orange precipitate. The product was filtered off, and washed with cold ethanol, and dried under vacuum. The final product was recrystallized from the DMF/ethanol mixture. Color: Orange. Yield: 66 %. m.p.: 253–255 °C. Anal. calcd for $C_{16}H_{13}N_5O_2S.C_3H_7NO$ (412.46 g/mol) (%): C 55.33, H 4.89, N 20.38, S 7.77; found (%): C 55.39, H 4.77, N 20.26, S 7.58. ^{1}H NMR (DMSO-d_6, 500 MHz) (δ, ppm): 14.57 (s, 1H, OH), 11.30 (s, 1H, isatin NH), 12.52 (s, 1H, NH), 10.11 (s, 1H, NH), 8.55 (s, 1H, CH = N), 7.95 (s, 1H, DMF CH = O), 8.11–6.86 (m, 8H, aromatic H), 2.89 (s, 3H, DMF CH_3), 2.73 (s, 3H, DMF CH_3). IR (cm^{-1}) (ν_{max}): 3223 (OH), 3165 and 3135 (NH), 1618 and 1586 (C═N), 1690 $(C{=}O)_{isatin}$, 1659 $(C{=}O)_{DMF}$, 1271 (C═S). UV–Vis (DMF) λ^{max} (nm): 264, 288, 368, 466.

2.2.3. Synthesis of 1-[2-oxoindolin-3-ylidene]-5-[5-bromo-2-hydroxyphenyl)methylidene]thiocarbohydrazone, H_2L2

The ligand, H_2L2, was prepared by the procedure as used for H_2L1 from 5-bromosalicylaldehyde (1 mmol) and 1-(2-oxoindolin-3-ylidene) thiocarbohydrazone (L) (1 mmol). Color: Orange. m.p.: 285–287 °C. Yield: 54 %. Anal. calcd for $C_{16}H_{12}BrN_5O_2S.C_3H_7NO$ (491.36 g/mol) (%): C 46.44, H 3.90, N 17.10, S 6.53; found: C 46.49, H 3.78, N 17.06, S 6.44. ^{1}H NMR (DMSO-d_6, 500 MHz) (δ, ppm): 14.54 (s, 1H, OH), 11.37 (s, 1H, isatin NH), 12.57 (s, 1H, NH), 10.48 (s, 1H, NH), 8.48 (s, 1H, CH = N), 7.94 (s, 1H, DMF CH = O), 8.19–6.87 (m, 7H, aromatic H), 2.88 (s, 3H, DMF CH_3), 2.72 (s, 3H, DMF CH_3). IR (cm^{-1}) (ν_{max}): 3219 (OH), 3174 and 3141 (NH), 1617 and 1591 (C═N), 1691 $(C{=}O)_{isatin}$, 1656 $(C{=}O)_{DMF}$, 1268 (C═S). UV–Vis (DMF) [λ^{max} (nm)]: 265, 287, 372, 463.

2.2.4. Synthesis of 1-[2-oxoindolin-3-ylidene]-5-[5-chloro-2-hydroxyphenyl)methylidene]thiocarbohydrazone, H_2L3

The ligand, H_2L3, was prepared by the procedure as used for H_2L1 from 5- chlorosalicylaldehyde (1 mmol) and 1-(2-oxoindolin-3-ylidene) thiocarbohydrazone (L) (1 mmol). Color: Orange. m.p.: 270–271 °C. Yield: 67 %. Anal. calcd for $C_{16}H_{12}ClN_5O_2S.C_3H_7NO$ (446.91 g/mol) (%): C 51.06, H 4.29, N 18.80, S 7.17; found: C 51.33, H 4.61, N 18.56, S

7.62. ^{1}H NMR (DMSO-d_6, 500 MHz) (δ, ppm): 14.57 (s, 1H, OH), 11.38 (s, 1H, isatin NH), 12.58 (s, 1H, NH), 10.45 (s, 1H, NH), 8.48 (s, 1H, CH = N), 7.95 (s, 1H, DMF CH = O), 8.09–6.93 (m, 7H, aromatic H), 2.89 (s, 3H, DMF CH_3), 2.73 (s, 3H, DMF CH_3). IR (cm^{-1}) (ν_{max}): 3211 (OH), 3171 and 3143 (NH), 1617 and 1590 (C═N), 1689 (C═O)$_{isatin}$, 1655 (C═O)$_{DMF}$, 1267 (C═S). UV–Vis (DMF) [λ^{max} (nm)]: 264, 288, 372, 456.

2.2.5. Synthesis of 1-[2-oxoindolin-3-ylidene]-5-[5-nitro-2-hydroxyphenyl)methylidene]thiocarbohydrazone, H_2L4

The ligand, H_2L4, was prepared by the procedure as used for H_2L1 from 5-nitrosalicylaldehyde (1 mmol) and 1-(2-oxoindolin-3-ylidene) thiocarbohydrazone (L) (1 mmol). Color: Orange. m.p.: 261–262 °C. Yield: 73 %. Anal. calcd for $C_{16}H_{12}N_6O_4S.C_3H_7NO$ (457.46 g/mol) (%): C 49.88, H 4.19, N 21.43, S 7.01; found: C 49.77, H 4.31, N 21.58, S 7.28. ^{1}H NMR (DMSO-d_6, 500 MHz) (δ, ppm): 14.61 (s, 1H, OH), 11.37 (s, 1H, isatin NH), 12.66 (s, 1H, NH), 11.77 (s, 1H, NH), 8.54 (s, 1H, CH = N), 7.95 (s, 1H, DMF CH = O), 8.89–6.93 (m, 7H, aromatic H), 2.89 (s, 3H, DMF CH_3), 2.73 (s, 3H, DMF CH_3). IR (cm^{-1}) (ν_{max}): 3213 (OH), 3168 and 3135 (NH), 1617 and 1574 (C═N), 1686 (C═O)$_{isatin}$, 1654 (C═O)$_{DMF}$, 1269 (C═S). UV–Vis (DMF) [λ^{max} (nm)]: 264, 289, 380, 481.

2.3. Synthesis of the complexes

2.3.1. Synthesis of 1-[2-oxoindolin-3-ylidene]-5-[2-hydroxyphenyl)methylidene]thiocarbohydrazone-triphenylphosphine-nickel(II), [NiL1(P)]

The Ni(II) complexes were prepared according to the method we used in our previous study as follows [18].

A solution of H_2L1 (1 mmol) was solved in DCM (10 mL) and ethanol (10 mL), followed by the addition of $NiCl_2{\cdot}6H_2O$ (1 mmol), and was refluxed for 1 h. The co-ligand of triphenylphosphine (1 mmol), was added to the solution. The mixture was refluxed for an additional 5 h. The resulting dark orange precipitate was filtered off, and washed with cold ethanol, and dried under vacuum. Color: Dark orange. m.p.: 224–225 °C. Yield: 49 %. Anal. calcd for $C_{34}H_{26}N_5NiO_2PS.C_2H_5OH$ (704.40 g/mol) (%): C 61.38, H 4.58, N 9.94, S 4.55; found: C 61.47, H 4.45, N 9.72, S 4.46. ^{1}H NMR (DMSO-d_6, 500 MHz) (δ, ppm): 13.21 (s, 1H, NH), 11.15 (s, 1H, isatin NH), 8.71 (s, 1H, CH = N), 7.77–6.33 (m, 23H, aromatic H), 3.44 (q, 2H, ethanol CH_2), 1.06 (t, 3H, ethanol CH_3). IR (cm^{-1}) (ν_{max}): 3231–3127 (NH), 1618 and 1601 (C═N), 1689 (C═O)$_{isatin}$; 1431, 1097, 742, 690 (PPh_3). UV–Vis (DMF) [λ^{max} (nm)]: 265, 280, 343, 414, 461.

2.3.2. Synthesis of 1-[2-oxoindolin-3-ylidene]-5-[5-bromo-2-hydroxyphenyl)methylidene]thiocarbohydrazone-triphenylphosphine-nickel(II), [NiL2(P)]

The complex, [NiL2(P)], was prepared according to procedure applied for [NiL1(P)] using H_2L2. Color: Dark orange. m.p.: 267–268 °C. Yield: 46 %. Anal. calcd for $C_{34}H_{25}BrN_5NiO_2PS.C_2H_5OH$ (783.29 g/mol) (%): C 55.20, H 3.99, N 8.94, S 4.09; found: C 55.52, H 3.61, N 8.56, S 4.47. ^{1}H NMR (DMSO-d_6, 500 MHz) (δ, ppm): 13.23 (s, 1H, NH), 11.16 (s, 1H, isatin NH), 8.73 (s, 1H, CH = N), 7.76–6.26 (m, 22H, aromatic H), 4.34 (s, 1H, OH), 3.44 (q, 2H, ethanol CH_2), 1.05 (t, 3H, ethanol CH_3). IR (cm^{-1}) (ν_{max}): 3236–3116 (NH), 1618 and 1597 (C═N), 1691 (C═O)$_{isatin}$; 1432, 1097, 741, 691 (PPh_3). UV–Vis (DMF) [λ^{max} (nm)]: 265, 279, 347, 417, 464.

2.3.3. Synthesis of 1-[2-oxoindolin-3-ylidene]-5-[5-chloro-2-hydroxyphenyl)methylidene]thiocarbohydrazone-triphenylphosphine-nickel(II), [NiL3(P)]

The complex, [NiL3(P)], was prepared according to procedure applied for [NiL1(P)] using H_2L3. Color: Dark orange. m.p.: 350>°C. Yield: 55 %. Anal. calcd for $C_{34}H_{25}ClN_5NiO_2PS.C_2H_5OH$ (738.84 g/mol) (%): C 58.52, H 4.23, N 9.48, S 4.34; found: C 58.60, H 4.32, N 9.54, S 4.38. ^{1}H NMR (DMSO-d_6, 500 MHz) (δ, ppm): 13.23 (s, 1H, NH), 11.17 (s, 1H, isatin NH), 8.73 (s, 1H, CH = N), 7.76–6.32 (m, 22H, aromatic H), 3.44 (q, 2H, ethanol CH_2), 1.06 (t, 3H, ethanol CH_3). IR (cm^{-1}) (ν_{max}): 3223–3119 (NH), 1619 and 1600 (C═N), 1673 (C═O)$_{isatin}$; 1432, 1097, 748, 691 (PPh_3). UV–Vis (DMF) [λ^{max} (nm)]: 265, 280, 348, 416, 465.

2.3.4. Synthesis of 1-[2-oxoindolin-3-ylidene]-5-[5-nitro-2-hydroxyphenyl)methylidene]thiocarbohydrazone-triphenylphosphine-nickel(II), [NiL4(P)]

The complex, [NiL4(P)], was prepared according to procedure applied for [NiL1(P)] using H_2L4. Color: Dark orange. m.p.: 293–294 °C. Yield: 62 %. Anal. calcd for $C_{34}H_{25}N_6NiO_4PS.C_2H_5OH$ (749.40 g/mol) (%): C 57.70, H 4.17, N 11.21, S 4.28; found: C 57.62, H 4.12, N 11.17, S 4.19. ^{1}H NMR (DMSO-d_6, 500 MHz) (δ, ppm): 13.31 (s, 1H, NH), 11.20 (s, 1H, isatin NH), 8.90 (s, 1H, CH = N), 7.69–6.20 (m, 22H, aromatic H), 3.37 (q, 2H, ethanol CH_2), 1.06 (t, 3H, ethanol CH_3). IR (cm^{-1}) (ν_{max}): 3195–3108 (NH), 1621 and 1599 (C═N), 1682 (C═O)$_{isatin}$; 1433, 1098, 744, 688 (PPh_3). UV–Vis (DMF) [λ^{max} (nm)]: 264, 280, 326, 406, 446.

2.4. X-ray crystallography

Single crystals suitable for XRD of H_2L1 and H_2L3 were obtained by slow evaporation at room temperature from the filtrate of crystallization solution (ethanol/DMF). Also, suitable complex crystals were grown by slow evaporation of the solution at room temperature from a mixture of DCM/propan-1-ol for [NiL1(P)] and DCM/propan-1-ol/DMF for [NiL3(P)].

Single crystal data were collected at room temperature on a Bruker APEX II CCD diffractometer equipped with graphite-monochromated Mo-Kα (λ = 0.71073 Å) radiation. Indexing, data reduction and absorption correction were performed using APEX2 suite [32]. Crystal structures were solved using SHELXT [33] and then refined by full-matrix least-squares refinements on F^2 using the SHELXL [34] in Olex2 (v.1.5) [35]. Crystallographic data and refinement parameters are given in Table 1. The aromatic and aliphatic C-bound H atoms were positioned geometrically and refined using a riding mode. The O—H and N—H distances were restrained to be 0.82 A and 0.86 from corresponding O/N atoms using DFIX, respectively and their positions were constrained to refine on their parent O atoms with Uiso(H) = 1.5Ueq(O) and Uiso(H) = 1.5Ueq(N). Additional crystallographic data with CCDC reference numbers 2,215,808 **(H_2L1)**, 2,215,809 **(H_2L3)**, 2,215,810 **[NiL1(P)]** and 2,215,811 **[Ni_3(L3)$_2$(P)$_2$]** has been deposited within the Cambridge Crystallographic Data Center *via* https://www.ccdc.cam.ac.uk/deposit. SQUEEZE [36] was used to eliminate the electron density of highly disordered solvent molecules in **[NiL1(P)]** and **[Ni_3(L3)$_2$(P)$_2$]** compounds.

2.5. Electrochemical studies

Electrochemical characterizations of the ligands and their complexes were determined by using Cyclic voltammetry (CV) technique with a Gamry Reference 600 potentiostat/galvanostat. All measurements were carried out in an electrochemical cell consisting of three electrode systems of a glassy carbon working electrode (GCE), a Pt wire counter electrode, and an Ag/AgCl reference electrode under nitrogen blanket at 25 °C [37]. Dimethyl sulfoxide (DMSO)/tetrabutylammonium perchlorate (TBAP) solution was used as the electrolyte for CV and *in situ* spectroelectrochemical measurements.

2.6. Measurement of antioxidant capacity using CUPRAC method

The antioxidant capacity of the ligands and complexes was measured by the CUPRAC method [38]. The CUPRAC assay is based on measuring the absorbance of the CUPRAC chromophore, Cu(I)-neocuproine (Nc) chelate, formed as a result of the redox reaction of antioxidants with the

Table 1
Crystal data and structure refinement for **H_2L1**, **H_2L3**, **[NiL1(P)]** and **[Ni_3(L3)$_2$(P)$_2$]**.

Identification code	H_2L1	H_2L3	[NiL1(P)]	[Ni_3(L3)$_2$(P)$_2$]
CCDC	2,215,808	2,215,809	2,215,810	2,215,811
Empirical formula	$C_{19}H_{20}N_6O_3S$	$C_{19}H_{19}ClN_6O_3S$	$C_{34}H_{26}N_5NiO_2PS$	$C_{74}Cl_2H_{64}N_{12}Ni_3O_7P_2S_2$
Formula weight	412.47	446.91	658.34	1606.46
Temperature/K	296.15	298	298	298
Crystal system	Triclinic	Monoclinic	Triclinic	Triclinic
Space group	*P*-1	$P2_1/n$	*P*-1	*P*-1
a/Å	9.854(7)	15.5022(12)	9.1944(16)	11.184(7)
b/Å	14.350(9)	13.3030(11)	13.836(2)	15.671(9)
c/Å	15.468(10)	21.5729(17)	15.195(3)	21.764(13)
α/°	92.984(11)	90	67.518(3)	106.443(9)
β/°	95.064(11)	107.6310(10)	75.983(3)	95.331(9)
γ/°	107.591(11)	90	88.771(3)	98.619(9)
Volume/Å^3	2070(2)	4239.9(6)	1727.5(5)	3580(4)
Z	4	8	2	2
ρ_{calc} (g/cm^3)	1.324	1.400	1.266	1.490
μ/mm^{-1}	0.189	0.312	0.704	1.022
F(000)	864.0	1856.0	680.0	1656.0
Crystal size/mm^3	0.22×0.18×0.13	0.424×0.27×0.268	0.342×0.065×0.055	0.172×0.116×0.076
Radiation	MoKα (λ = 0.71073)	MoKα (λ = 0.71073)	MoKα (λ = 0.71073)	MoKα (λ = 0.71073)
2Θ range for data collection/°	2.652 to 49.988	2.866 to 49.998	3.196 to 50	2.756 to 49.998
Index ranges	$-11 \le h \le 11$, $-17 \le k \le 17$, $-18 \le l \le 18$	$-18 \le h \le 18$, $-15 \le k \le 15$, $-25 \le l \le 25$	$-10 \le h \le 10$, $-16 \le k \le 16$, $-18 \le l \le 18$	$-13 \le h \le 13$, $-18 \le k \le 18$, $-25 \le l \le 25$
Reflections collected	19,519	37,462	21,672	54,384
Independent reflections	7290 [R_{int} = 0.0631, R_{sigma} = 0.0783]	7463 [R_{int} = 0.0378, R_{sigma} = 0.0287]	6062 [R_{int} = 0.0459, R_{sigma} = 0.0461]	12,616 [R_{int} = 0.0900, R_{sigma} = 0.0877]
Data/restraints/parameters	7290/24/529	7463/0/547	6062/294/397	12616/0/820
Goodness-of-fit on F^2	0.968	1.064	1.110	1.068
Final R indexes [I>=2σ (I)]	R_1 = 0.0570, wR_2 = 0.1394	R_1 = 0.0392, wR_2 = 0.0949	R_1 = 0.0597, wR_2 = 0.1463	R_1 = 0.0732, wR_2 = 0.1828
Final R indexes [all data]	R_1 = 0.1337, wR_2 = 0.1640	R_1 = 0.0659, wR_2 = 0.1050	R_1 = 0.0795, wR_2 = 0.1539	R_1 = 0.1149, wR_2 = 0.1948
Largest diff. peak/hole/e Å^{-3}	0.35/-0.21	0.18/-0.20	0.78/-0.78	0.84/-0.72

CUPRAC reagent, bis(neocuproine) copper(II) cation (Cu(II)-Nc).

1 mL of aqueous $CuCl_2{\cdot}2H_2O$ (10^{-2} M) solution, 1 mL of ethanolic neocuproine solution (7.5x10^{-3} M) and 1 mL of aqueous NH_4Ac buffer (1 M) solution (at pH 7) were added into a test tube, respectively. An antioxidant sample solution (x mL) and distilled water (1.1-x mL) were then added to these tubes. The tubes (total volume 4.1 mL) were stoppered, and after 30 min, the absorbance at 450 nm was recorded against a reagent blank. From the absorbance versus concentration graph, the standard calibration curve of each compound was obtained. The molar absorptivity for each compound was found from the slope of the calibration line concerned. TEAC (Trolox equivalent antioxidant capacities) coefficients of the compounds were calculated by the ratio of the molar absorptivity of each compound to that of Trolox. All determinations were repeated at least three times. Obtained data are presented as averaged value ± standard deviation (SD).

2.7. Measurement of antioxidant activity using DPPH method

The DPPH radical scavenging activity of the ligands was determined according to the methodology of Brand-Williams et al. with minor modifications [39]. In this method, DPPH radical solution (2 mL, 10^{-4} M) in ethanol, sample solution (1 mL, 10^{-4} M) in ethanol and ethanol (1 mL) were rapidly added to a test tube in this order. The mixture (total volume 4 mL) was incubated in a dark place for 30 min at room temperature and then absorbance was measured at 515 nm against ethanol. A mixture of ethanol (2 mL) and DPPH• solution (2 mL) was used as the control solution. Test compounds were compared with the standard, Trolox. The percentage of DPPH scavenging activity of the ligands (%) was calculated by use of the following equation:

DPPH radical scavenging activity (%) = [(A – B)/A] × 100, where A is the absorbance of the control and B is absorbance of the samples.

3. Results and discussion

3.1. Synthesis and spectral characterization

Novel asymmetric bisthiocarbohydrazone ligands (H_2L1-H_2L4) were synthesized by the reaction of 1-(2-oxoindolin-3-ylidene)thiocarbohydrazone (L) and respective 5-substituted salicylaldehydes in ethanol-DMF (Scheme 1). The ligands are very soluble in acetone, DCM, DMSO and DMF. The mixed ligand Ni(II) complexes {[NiL1(P)]-NiL4(P)]} were obtained from the reaction of the ligands with $NiCl_2{\cdot}6H_2O$ in the presence of triphenylphosphine (P) under reflux condition (Scheme 1). Asymmetric bisthiocarbohydrazones acted as a dibasic tridentate ligand. The complexes dissolve in chloroform, acetone, DCM, DMF and DMSO. The analytical data of the complexes confirmed the proposed molecular formula.

The molar conductivity values of the complexes at 10^{-3} M DMSO are in the range of 15–22 Ω^{-1} cm^2 mol^{-1}, indicating that the complexes are not electrolytes [18,40].

The μ_{eff} measurements showed that the complexes are diamagnetic and revealed the square planar geometry of the low spin nickel(II) ion [18,37].

UV–Vis spectra of the ligands and complexes were recorded in DMF (3×10^{-5} M) solution at room temperature. In all bisthiocarbohydrazone ligands, the bands at 264–265 nm and 287–289 nm involve π → π* transitions related to the aromatic ring. In the complexes, these bands are seen around 265 nm and 280 nm. Bands between 368 and 380 nm and 456–481 nm can be attributed to the n → π* transitions of thioamide moiety and azomethine group in the ligands. In the complexes, observation of the shifting to the lower wavelength of these bands (326–348 nm and 406–417 nm) supports the coordination to the metal through thioamide moiety and azomethine group of the ligands. In addition, the Ni(II) complexes show absorption bands which can be attributed to the

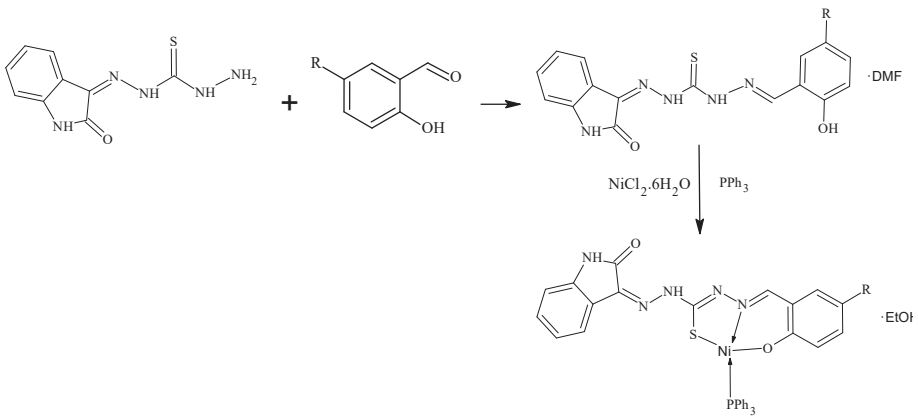

Scheme 1. General synthesis of the ligands and complexes {H_2L1 and [NiL1(P)]: (R = H), H_2L2 and [NiL2(P)]: (R = Br), H_2L3 and [NiL3(P)]: (R = Cl), H_2L4 and [NiL4(P)]: (R = NO_2)]}.

charge transfer transition at 446–465 nm [18,27,41]. UV–vis spectra of the ligands and complexes are given in Figs. S1 and S2.

IR and ^{1}H NMR spectra of the complexes were compared with those of the ligands in order to find out the points of attachment of the ligands to the metal ion in the complexes.

In the IR spectra, the phenolic ν(OH) vibration bands of the ligands appear around 3200 cm^{-1}. These bands disappeared in the complexes. This indicates the complexation occurs via deprotonation of the OH group. The ν(C═N) bands observed at 1618 and 1586 cm^{-1} for H_2L1, 1617 and 1591 cm^{-1} for H_2L2, 1617 and 1590 cm^{-1} for H_2L3, 1617 and 1574 cm^{-1} for H_2L4 shifted in all complexes, which confirm the coordination of azomethine nitrogen. The ν(C═S) bands appearing around 1270 cm^{-1} in the ligands disappeared on complexation. This indicates the coordination of S atom to the nickel ion. Finally, in the spectra of all complexes, the bands corresponding to triphenylphosphine were observed around 1432, 1097, 742 and 690 cm^{-1} [18,37,42,43]. IR spectra of the ligands and complexes are given in Figs. S3-S10.

In the ^{1}H NMR spectra of the ligands; OH protons were observed as singlets at 14.57 ppm for H_2L1, 14.54 ppm for H_2L2, 14.57 ppm for H_2L3 and 14.61 ppm for H_2L4. The absence of these bands in the complexes suggests that ligands coordinate to metal atom through oxygen atom by deprotonation. In the ligands, the signals attributed to the NH group of isatin are seen as singlets in the range of 11.30–11.38 ppm. The appearance of these NH peaks at almost the same place in the complexes (11.15–11.20 ppm) proves that the isatin part of the ligands is not involved in the formation of the complex. The peaks belonging to the

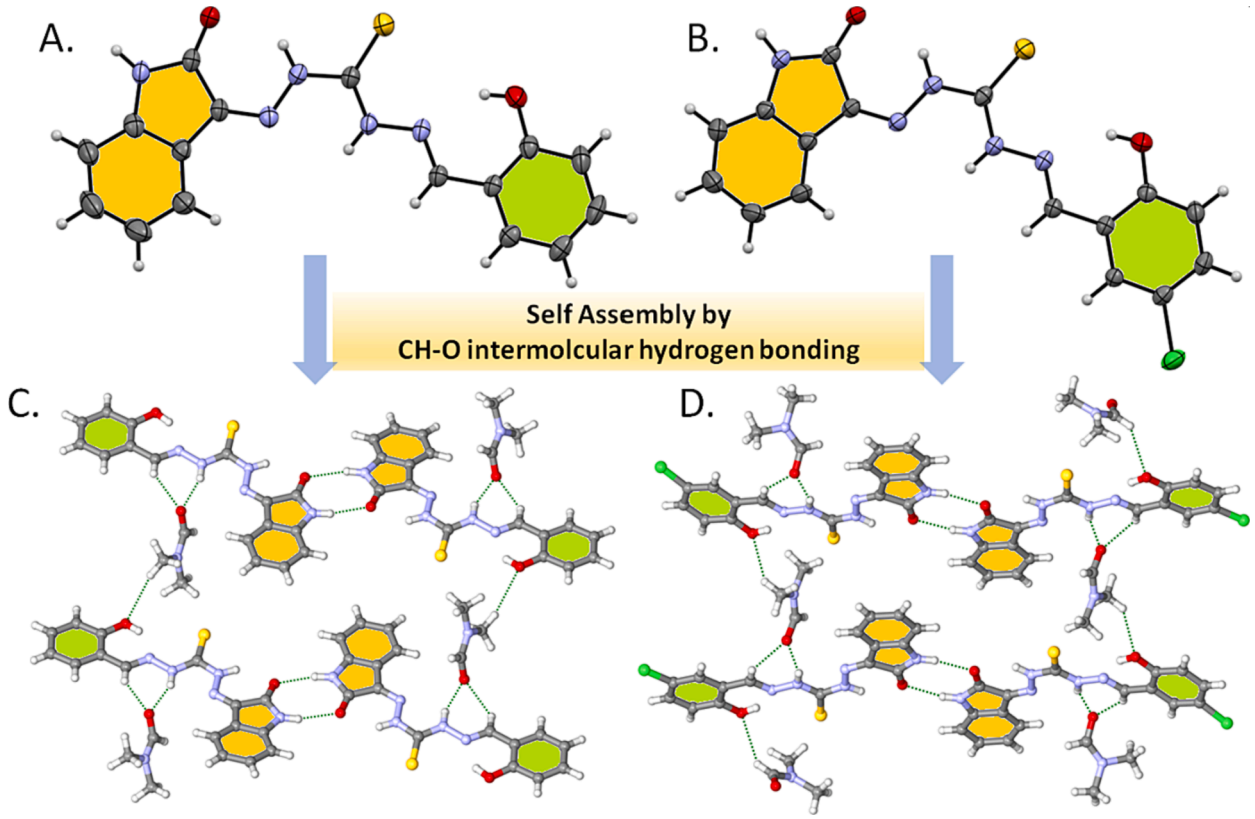

Fig. 1. ORTEP drawings (30 % probability level) of the crystal structure of **H_2L1** (A) and **H_2L3** (B). All hydrogen atoms and DMF molecules are omitted for clarity in the lattices. C. and D. Perspective view of the CH···O and NH···O hydrogen bonding interactions between DMF solvate and molecules (**H_2L1** and **H_2L3**) as green dotted lines.

two NH groups of thiocarbohydrazide appear at 12.52 and 10.11 ppm, 12.57 and 10.48 ppm, 12.58 and 10.45 ppm, 12.66 and 11.77 ppm in the ligands H_2L1, H_2L2, H_2L3 and H_2L4, respectively. In the complexes, the appearance of only one of these NH peaks (around 13.25 ppm) can be interpreted that only one of N atoms is bonded to the metal by deprotonation. In addition, the presence of DMF in the ligands and ethanol in the complexes was clearly observed in the NMR spectra [18,37,44,45]. ^{1}H NMR spectra of the ligands and complexes are given in Figs. S11-S18.

3.2. Crystal structures descriptions

In order to gain more insight into the solid state structure, single crystal X-ray diffraction analysis was used to unambiguously elucidate compounds **H_2L1**, **H_2L3**, **[NiL1(P)]**, and **$[Ni_3(L3)_2(P)_2]$**. Table 1 provides X-ray crystallographic data as well as data collecting refinement information. Single crystal X-ray diffraction analysis revealed that **H_2L1** and **H_2L3** crystallize in the triclinic space group *P*-1 and monoclinic space group $P2_1/n$, in which the asymmetric unit consists of two crystallographically distinct DMF solvate and molecules (**H_2L1** and **H_2L3**, Fig. 1A and B). **H_2L1** and **H_2L3** display a substantially planar molecular configuration with quite small dihedral angles, in which the 2-oxoindolin-3-ylidene subunit and the phenyl ring (5.58° and 1.94° for **H_2L1**, 3.65° and 13.68° for **H_2L3**). The N—N [1.375(3) Å – 1.348(3) Å/1.368 (3) Å – 1.347(3) Å for **H_2L1**; 1.353(2) Å – 1.367(3) Å/1.347(2) Å – 1.369(3) Å for **H_2L3**] bond distances fall somewhere between the ideal N—N and N═N bond distances, indicating electron delocalization through the entire thiocarbohydrazone moiety. The C—S bond lengths are found to be 1.647(3) Å – 1.650(3) for **H_2L1** and 1.650(3) Å – 1.654 (3) for **H_2L3**, which are close to C═S double bond distance in the literature [18,46]. Both molecules exist in E-Z configuration around the C═N as shown in C7-N1/C9-N4 for **H_2L1** and *C*2-N4/C15-N2 for **H_2L3**. In **H_2L1**, the intermolecular C—H···O (C34···O1 = 3.586 Å, C26···O6 = 3.221 Å), N—H···O (N7···O2 = 2.845 Å, N5···O23 = 2.908 Å) and C—H···S (C38···S2 = 3.621 Å) hydrogen bonding interactions lead a one-dimensional hydrogen-bonded chain (Fig. 1C). The intermolecular C—H···O (*C*2···O6 = 3.166 Å, C38···O1 = 3.359 Å, C18···O5 = 3.130 Å) and N—H···O interactions (N3···O6 = 2.820 Å, N10···O2 = 2.907 Å, N5···O4 = 2.873 Å, N8···O5 = 2.925 Å) primarily stabilize the crystal structure of **H_2L3** (Fig. 1D).

[NiL1(P)] crystallizes in the triclinic *P*-1 space group. As shown in Fig. 2A, the asymmetric unit cell of **[NiL1(P)]** consists of one ligand **(H_2L1)**, one Ni(II) metal cation, and one triphenylphosphine (PPh_3). Three donor atoms (S1, O1, N1) of **H_2L1** and one phosphorous atom (*P*1) of PPh_3 coordinated the Ni(II) metal center to form a distorted square planar coordination geometry. The nearly planar thiocarbohydrazone ligand **(H_2L1)** with Ni(II) cation forms six- and five-membered chelate rings with O1-Ni1-N1 (95.13°) and S1-Ni1-N1 (87.64°) angles, respectively, and these angles are consistent with those seen in similar Ni(II) coordination geometry [47,48]. The bond lengths in the Ni(II) coordination sphere of **[NiL1(P)]** are 1.871(3) Å for Ni1-N1, 1.841(3) Å for Ni1-O1, and 2.2013(12) Å for Ni1-*P*1 and 2.1308(12) Å for Ni1-S1, which agree with the literature report [18]. The intermolecular CH···π interactions help to form a three-dimensional supramolecular network (Fig. 2B). **$[Ni_3(L3)_2(P)_2]$** was obtained by crystallization of **[NiL3(P)]** in a solvent mixture of DCM/propan-1-ol/DMF. Crystallographic analysis revealed that **$[Ni_3(L3)_2(P)_2]$** crystallizes in the triclinic crystal system with space group *P*-1. As can be seen in Fig. 3A, the compound exhibits a trinuclear metal complex with the asymmetric unit containing cry-stallographically-three distinct Ni(II) metal cations, two ligands and two triphenylphosphines (PPh_3). The Ni1 and Ni3 metal cations have a square planar coordination geometry built up by N1, O4, S2 and N6, O1, S1 donor atoms from two ligands **(H_2L3)**, respectively. The triphenylphosphine ligand completes the metal atom's fourth coordination. The trinuclear metal complex is made by the octahedral coordination of the third Ni(II) metal center, which is coordinated with two oxygen atoms (O2, O3) from 2-oxoindolin-3-ylidene moieties and four nitrogen atoms (N2, N4, N7, N9) from thiocarbohydrazones. The average bond lengths of **$[Ni_3(L3)_2(P)_2]$** around the square planar Ni(II) metal center are 1.885 Å for Ni-N, 1.830 Å for Ni-O, and 2.210 Å for Ni1-*P*1, which seem to be coherent with those found in **[NiL3(P)]**. On the other hand, the Ni-N and Ni-O bond distances around the octahedral Ni(II) metal center are between 2.069(5) Å – 2.100(5) Å and 2.185(5) Å – 2.211(5) Å. Three dimensional supramolecular network (Fig. 3B) is stabilized by the short range intermolecular π···π, Cl···π, and CH···π interactions.

3.3. Electrochemical studies

Redox activities of the ligands and nickel(II) complexes were determined with CV in DMSO/TBAP electrolyte systems. All voltammograms recorded at various scan rates are represented in the supplementary material file (Figs. S19-S26). All voltammograms were analyzed and derived half wave potentials are tabulated in Table 2. The CVs of the ligands are represented in Fig. 4. As shown in this figure, four quasi reversible reduction and one irreversible oxidation processes are recorded for all ligands and there are small potential shifts in these processes due to the different substituents on the ligands. The most easily reduced one is **H_2L4** and the hardest reducing ligand is the **H_2L1**. In order to perform detailed analyses of the redox couples, CVs are recorded with different scan rates and vertex potentials. Influences of the vertex potential to the redox mechanism of **H_2L4** are given as an

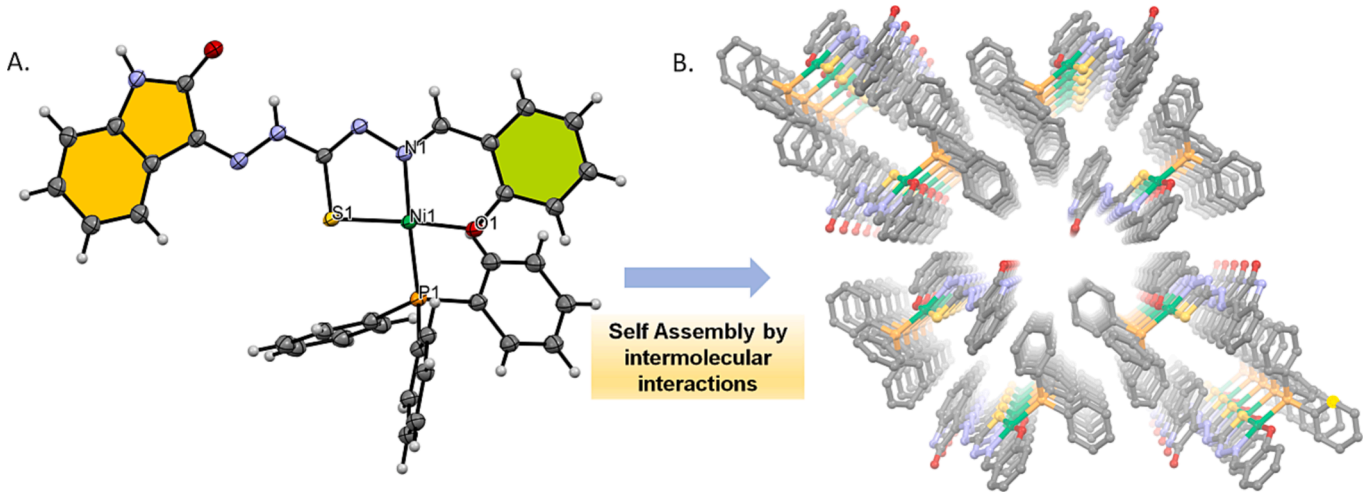

Fig. 2. ORTEP drawing (30% probability level) of the crystal structure of **[NiL1(P)]** (A) and crystal packing illustration of **[NiL1(P)]** (B).

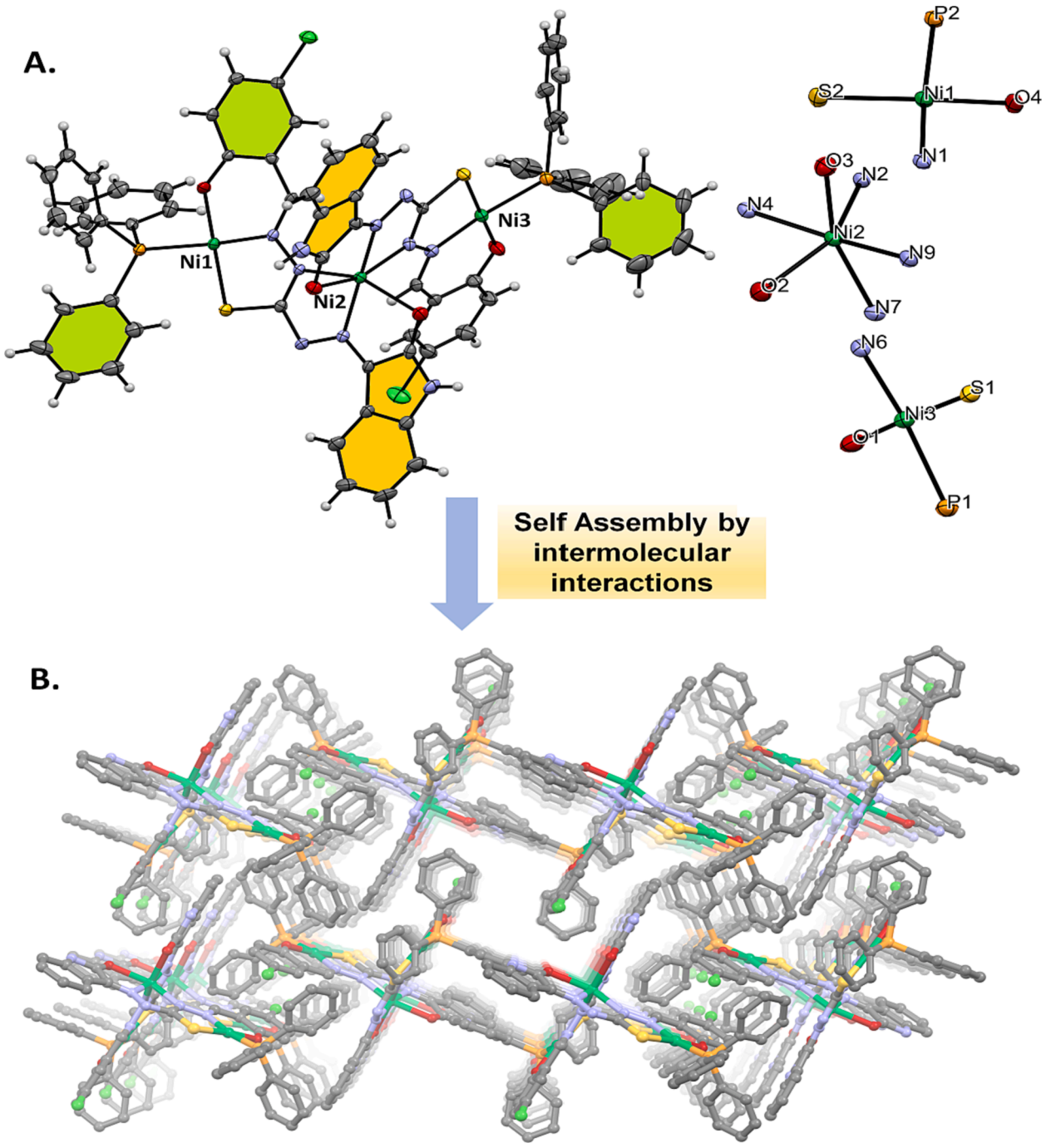

Fig. 3. ORTEP drawing (30% probability level) of the crystal structure of **[Ni_3(L3)$_2$(P)$_2$]** (A) and crystal packing illustration of **[Ni_3(L3)$_2$(P)$_2$]** (B).

example in Fig. 5. As shown in this figure when the cathodic vertex potentials gradually shift towards the negative potentials, some couples disappear, and new anodic waves are observed. During the first CV cycle between 0 and −1.0 V, a cathodic wave is recorded at −0.94 V. This wave gradually disappears when the vertex potential increases. Same trend is recorded for the second reduction wave at −1.17 V. With the consequent CVs, the waves at −0.94 and −1.17 V completely disappear and only two waves −1.50 and −2.07 V remain as unchanged. Moreover, new anodic waves are observed at −0.97, −0.52, and 0.04 V during the reverse scan of the CV which is returned back from −2.50 V. These redox finding shows chemical irreversibility of the electron transfer reactions. Although the **H_2L4** illustrates chemically irreversible character, stable oxidation waves are observed for all CVs having different vertex potentials. Similar chemical irreversibilities of the reduction processes are also observed with other ligands with different chemical reaction rates.

The formation of Ni(II) complexes **{ [NiL1(P)] - [NiL4(P)] }** with the corresponding ligands does not considerable influence the reduction processes as shown in Fig. 6. All complexes illustrate similar redox responses with those of the corresponding ligands. Reduction waves of the complexes slightly shift towards negative potentials with respect to the ligands. Differently, a metal-based oxidation wave is observed before the ligand oxidation waves as shown in Fig. 6. Redox mechanisms of the complexes are analyzed with the repetitive CVs having different vertex potentials. As represented in Fig. 7, the presence of the chemical reactions after the redox waves are clearly observed with the disappearing

Table 2
Voltammetric data of the compounds.

Compounds	Redox processes ([a]E_p vs Ag/AgCl (V))						Ref.
	Ligand oxd.	Ni^{II}/Ni^{III}	Ligand red.'s				
L1*	1.03	–	−0.77	−1.17	−1.50	–	[18]
L2*	1.18	–	−0.80	−1.20	−1.53	−2.00	[18]
L3*	1.15	–	−0.74	−1.13	−1.44	−1.90	[18]
C1*	1.10	0.79	−0.93	−1.24	−1.74	−2.02	[18]
C2*	1.07	0.77	−0.89	−119	−1.78	−2.08	[18]
C3*	1.06	0.79	−0.76	−1.15	−1.46	−1.92	[18]
H_2L1	1.08	–	−0.92	−1.28	−1.47	−1.75	tw
H_2L2	1.07	–	−0.99	−1.33	−1.61	−2.02	tw
H_2L3	1.03	–	−0.98	−1.34	−1.63	−2.03	tw
H_2L4	1.13	–	−0.95	−1.16	−1.50	−2.06	tw
[NiL1(P)]	1.30	1.00	−1.08	−1.27	−1.48	−1.73	tw
[NiL2(P)]	1.27	1.08	−1.10	−1.22	−1.80	−2.13	tw
[NiL3(P)]	1.28	1.04	−1.09	−1.28	−1.64	−1.94	tw
[NiL4(P)]	1.04	1.00	−1.04	−1.24	−1.61	−2.04	tw

[a] E_{pc} and E_{pa} values were given for the reduction and oxidation processes respectively.

* These compounds are thiocarbohydrazones (L1, L2, L3) and their nickel(II) complexes (C1, *C*2, C3) obtained from isatin and halogen disubstituted salicylaldehydes we synthesized in the previous study [18].

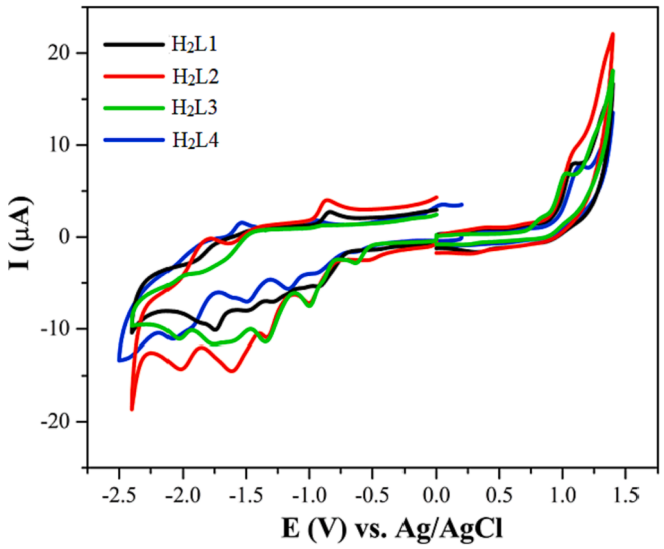

Fig. 4. CV responses of the ligands **H_2L1-H_2L4** at 100 mVs^{-1} scan rate on a GCE electrode in DMSO/TBAP.

the first two reduction couples when the vertex potentials go to more negative potentials. These voltammetric findings indicate that chemical irreversibilities of the redox processes of the ligands are still present after the complexation with Ni(II) ions. As shown in Table 2, when we compared these responses with the Ni(II) complexes (C1-C3) of the ligands (L1-L3) having 3,5-disubstituted salicylaldehydes [18], it is clearly shown that while oxidation potentials shift towards more positive potentials the reduction processes shift toward the more negative potentials. These data show increasing the HOMO LUMO gap of obtained complexes **{[NiL1(P)]-NiL4(P)]}** by using halogen monosubstituted salicylaldehydes with respect to the disubstituted counterparts (C1-C3). Moreover, the Ni(II) complexes of salicylaldehydes published by our group illustrated Ni(II)/Ni(III) oxidation processes between 0.77 and 0.79 V [18]. Ni(II)/Ni(III) oxidation process for the various Ni(II) Schiff base complexes was also reported in the literature by other groups [49–51]. For example, A.H. Kianfar et al. reported Ni(II)/Ni(III) oxidation couples between 0.70 and 1.06 V for the four different Ni(II) unsymmetrical N_2O_2 Schiff base complexes [49]. In

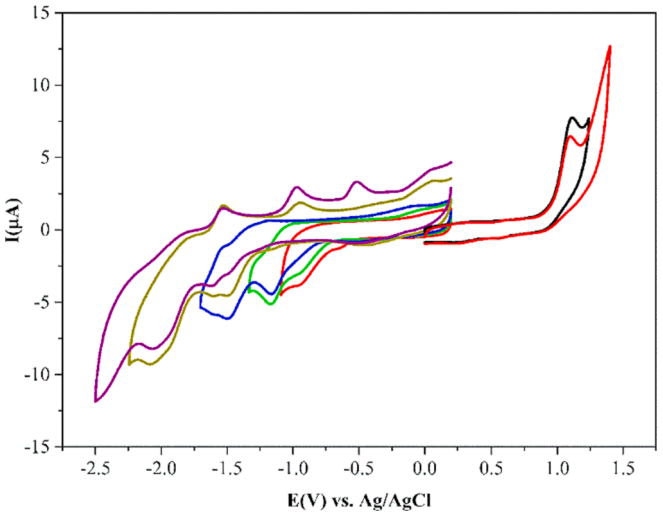

Fig. 5. Switchable CV responses of **H_2L4** at 100 mVs^{-1} scan rate on a GCE electrode in DMSO/TBAP.

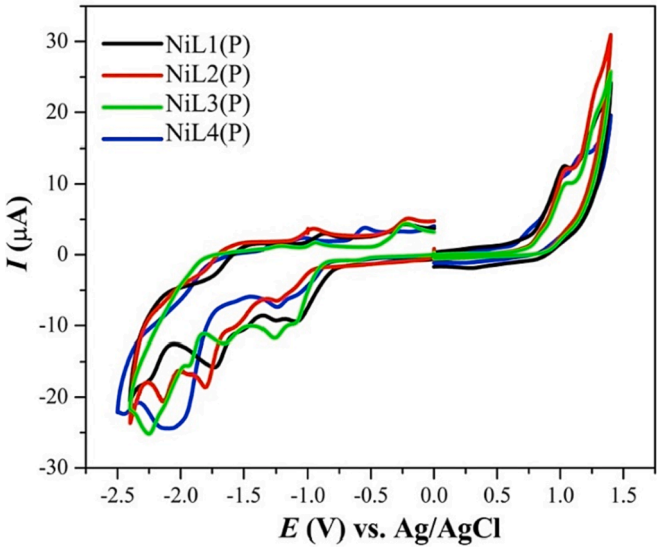

Fig. 6. CV responses of the complexes **[NiL1(P)]-[NiL4(P)]** at 100 mVs^{-1} scan rate on a GCE electrode in DMSO/TBAP.

another study, B. Bouzerafa et al. investigated the electrochemistry of Ni (II)-2L (L: ethane 2-(4-methoxyphenyl)-1-iminosalicylidene) complex on the GC-electrode in DMF solutions and reported a Ni(II)/Ni(III) oxidation process at 0.75 V [50]. L.-Q. Chai reported a Ni(II)/Ni(III) couple at 0.90 V for the Schiff base-type Ni(II) complex, $[Ni(L^2)_2]\cdot CH_3OH$ (HL^2 = 1-(2-{[(*E*)-3,5-dibromo-2-hydroxybenzylidene]amino} phenyl)ethanone oxime) in DMF/TBAP vs Ag/AgCl [51]. When we compare our results with the relevant literature, we could easily assign the first oxidation couples of all **{[NiL1(P)]-NiL4(P)]}** complexes to the Ni(II)/Ni(III) process. The redox mechanisms of the ligands and their nickel complexes are also supported by the *in situ* spectroelectrochemical measurements discussed below.

3.4. *In situ spectroelectrochemical studies*

In situ spectroelectrochemical measurements were carried out to investigate the spectral responses of the neutral and anionic and cationic forms of the H_2L and [NiL(P)] moieties. All ligands illustrate similar responses, thus *in situ* spectroelectrochemical result of **H_2L3** is

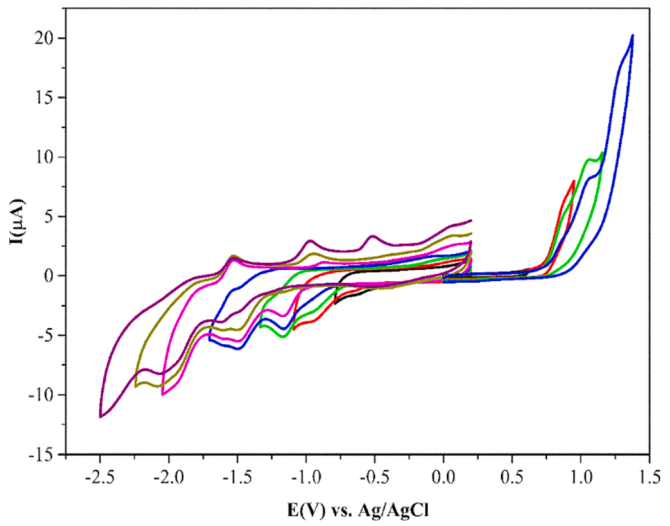

Fig. 7. Switchable CV responses of **[NiL3(P)]** at 100 mVs^{-1} scan rate on a GCE electrode in DMSO/TBAP.

represented in Fig. 8, **H_2L3** represents three bands between 325, 395, and 432 nm which are resulted from π-π* and n-π* transitions [52]. All H_2L species give near spectra in their neutral forms. During the electrolysis of the electrolyte at −120 V, while the band at 432 nm increases, a new broad band is observed at 472 nm. Moreover, while the band at 395 nm remains unchanged, a novel band at 287 nm is recorded (Fig. 8a). Similar trend in the spectral changes continues under −2.40 V potential application (Fig. 8b). In addition to the previous changes, a new broad band at 500 nm is enhanced in addition to the band at 472 nm. Up on 1.30 V potential application, a slight increase in the intensity of the band at 432 nm is only recorded, while the other bands do not change in intensity (Fig. 8c). All of these spectral changes are consistence with the ligand-based reductions of similar ligands published [26,53–55]. Pronounce color changes with respect to similar species in the literature are first reported during the spectral changes of **H_2L3** in this study. As shown in the chromaticity diagram in Fig. 8d, yellow color (x = 0.378; y = 0.408) of the neutral **H_2L3** turns to dark orange (x = 0.476; y = 0.456) and then to deep red (x = 0.512; y = 0.417) after the reduction reactions and turns to deep yellow (x = 0.420; y = 0.467) after the oxidation process. These spectral changes indicate possible usage of the ligand in the display technologies.

Complexation of the ligands with Ni(II) cation considerably alter the spectral changes with respect to the corresponding ligands. All Ni(II) complexes show similar spectral changes thus, the responses of **[NiL3 (P)]** are given in Fig. 8 as an example. Under −1.85 V potential application, while the bands of neutral **[NiL3(P)]** at 350 and 391 nm, three new bands are observed at 435, 472, and 573 nm. Moreover, the band at 268 nm increases in intensity (Fig. 9a). Although the general trends of the spectral changes are similar to those of **H_2L3**, the intensity of the new bands of **[NiL3(P)]** is more than the ligand. Under −2.40 V applied potential, two new bands are observed at 550 and 580 nm (Fig. 9b). Spectral changes given in Fig. 9c recorded during the oxidation of **[NiL3 (P)]** are completely different than those of **H_2L3**, which indicates metal based character of the first oxidation process of **[NiL3(P)]** . As shown in Fig. 9c, two new bands are recorded at 437 and 472 nm due to the formation of Ni(III)L3(P) due to the oxidation of Ni(II)L3(P). These

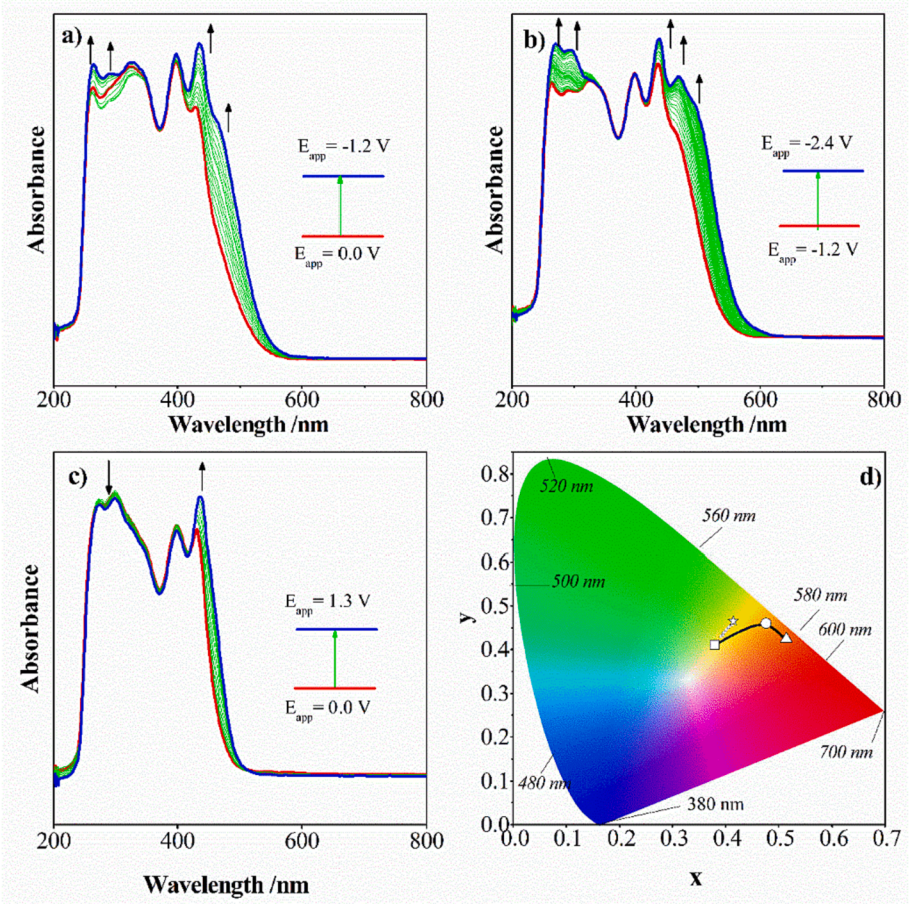

Fig. 8. In-situ UV–Vis spectral changes of **H_2L3** observed during the redox reactions in DMSO/TBAP electrolyte system, **a)** E_{app} = -1.25 V, **b)** E_{app} = -2.40 V, **c)** E_{app} = 1.30 V and **d)** Chromaticity diagram (each symbol represents the color of electro-generated species; □: **H_2L3**; ○: color at −1.25 V; △:color at −2.40 V; ★: 1.30 V.

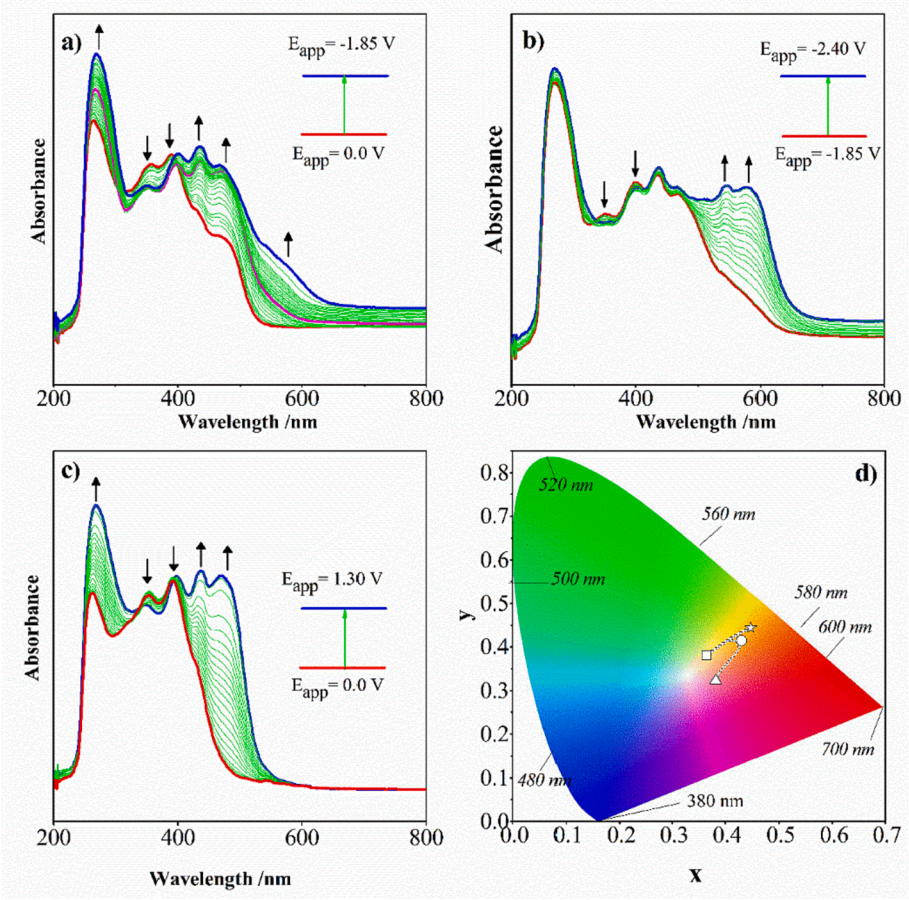

Fig. 9. In-situ UV–Vis spectral changes of **[NiL3(P)]** observed during the redox reactions in DMSO/TBAP electrolyte system, **a)** E_{app} = -1.85 V, **b)** E_{app} = -2.40 V, **c)** E_{app} = 1.30 V and **d)** Chromaticity diagram (each symbol represents the color of electro-generated species; □: **[NiL3(P)]** ; ○: color at −1.25 V; △:color at −2.40 V; ★: 1.30 V.

distinct spectral changes cause prominent color changes [26,53–55]. As shown in Fig. 9d, the yellow color (x = 0.360; y = 0.379) of the neutral **[NiL3(P)]** complex changes to orange (x = 0.424; y = 0.411) and then to pink (x = 0.381; y = 0.316). Similarly, orange color (x = 0.447; y = 0.448) is obtained after the oxidation process. These valuable color changes indicate the possible functionality of the complex as a chromophore between different color changes.

3.5. Antioxidant capacity

The ligands and their Ni(II) complexes were screened for their antioxidant capacity using the CUPRAC method [38]. The TEAC values of the compounds are given in Table 3. When the values are examined, it is seen that all the compounds show higher antioxidant activity than Trolox ($TEAC_{trolox}$: 1). In addition, the complexes have higher antioxidant capacity than the ligands [18].

3.6. FRS activity of the ligands

The free radical scavenging (FRS) activities of the ligands were calculated as percentage inhibition (Table 4). The ligands exhibit low radical scavenging activity compared to Trolox. FRS activities of the complexes at the same solvent and concentration could not be tested because their absorbance values were out of scale.

4. Conclusion

The Ni(II) mixed ligand complexes were prepared of the new bisthiocarbohydrazones derived from isatin monothiocarbohydrazone and 5-substituted salicylaldehydes. The synthesized ligand and complexes were characterized by elemental analyses, ^{1}H NMR, IR and electronic spectroscopy and conductivity measurements. The bisthiocarbohydrazones (H_2L1-H_2L4) act as tridentate ligands and form square planar Ni(II) complexes {[NiL1(P)-NiL4(P)]}. The fourth coordination is

Table 3
The TEAC coefficients of the compounds with respect to the normal CUPRAC assay (Trolox ε_N: 1.67×10^4 L mol^{-1} cm^{-1}).

Compounds	Molar absorptivity (L mol^{-1} cm^{-1})	$TEAC_{CUPRAC}$	Correlation coefficient (r)
L	1.6035×10^4	0.96 ± 0.077	0.9990
H_2L1	2.8194×10^4	1.69 ± 0.064	0.9998
H_2L2	3.0552×10^4	1.83 ± 0.175	0.9986
H_2L3	3.1023×10^4	1.86 ± 0.100	0.9995
H_2L4	2.0279×10^4	1.21 ± 0.206	0.9957
[NiL1(P)]	4.0866×10^4	2.45 ± 0.249	0.9984
[NiL2(P)]	4.6013×10^4	2.75 ± 0.502	0.9951
[NiL3(P)]	5.4746×10^4	3.28 ± 0.259	0.9990
[NiL4(P)]	3.5191×10^4	2.11 ± 0.346	0.9960

Table 4
The radical scavenging activities of the ligands (initial concentration: 10^{-4} M; sample volume: 1 mL).

Compounds	% FRS activity
L	3.40 ± 0.44
H_2L1	24.60 ± 0.98
H_2L2	25.50 ± 1.80
H_2L3	28.88 ± 2.47
H_2L4	8.79 ± 1.53
Trolox	95.37 ± 0.88

completed by monodentate ligand, PPh_3.

Single crystal structures of H_2L1 and H_2L3 ligands, [NiL1(P)] and [NiL3(P)] complexes were resolved by X-ray diffraction method. The crystal structure studies of new bisthiocarbohydrazone ligands derived from mono-substituted salicylaldehydes and isatin can be seen as an exemplary study. In addition, two different structures were obtained depending on the solvent in Ni(II) complexes containing triphenylphosphine. The [NiL1(P)] complex exhibits a crystalline structure compatible with the solid complex and crystallized as a monomer. By dissolving the [NiL3(P)] solid complex in a different solvent mixture and keeping it waiting, a completely new trinuclear Ni(II) complex, $[Ni_3(L3)_2(P)_2]$, also containing triphenylphosphine, was obtained. Despite interpretations that bulky ligands such as triphenylphosphine generally inhibit dimeric structures, a very interesting trinuclear species has emerged, containing Ni(II) ions with three different environments. Polynuclear transition metal complexes will be of interest to today's researchers as pioneering compounds in producing new magnetic materials and describing different biological processes.

Ligands and complexes showed higher antioxidant capacity than Trolox. Ligand H_2L2 has the highest radical scavenging activity among the synthesized ligands.

Electrochemical responses of the ligands and their Ni(II) complexes supported the proposed structures, thus proving the successful synthesis of the compounds. Multi-electron redox reactions of all compounds showed their values in various electrochemical applications. Spectral and color changes under applied potentials indicated their possible usages as electrochromic materials in various fields.

Declaration of Competing Interest

The authors declare that they have no known competing financial interests or personal relationships that could have appeared to influence the work reported in this paper.

Data availability

No data was used for the research described in the article.

Acknowledgements

This work was supported by the Scientific Research Projects Coordination Unit of Istanbul University-Cerrahpaşa (Project Number FBA-2017-25859).

Appendix A. Supplementary data

Supplementary data to this article can be found online at https://doi.org/10.1016/j.ica.2023.121403.

References

[1] M.H. Assaleh, A.R. Božić, S. Bjelogrlić, M. Milošević, M. Simić, A.D. Marinković, I. N. Cvijetić, Struct. Chem. 30 (2019) 2447–2457.
[2] F. Kurzer, M. Wilkinson, Chem. Rev. 70 (1970) 111–149.
[3] C. Bonaccorso, T. Marzo, D. La Mendola, Pharmaceuticals 13 (2020) 1–19.
[4] A.A. Abu-Hussen, A.A. Emara, J. Coord. Chem. 57 (2004) 973–987.
[5] I.S. Luna, W.W. Neves, R.G.d. Lima-Neto, A.P.B. Albuquerque, M.G.R. Pitta, M.J.B. M. Rêgo, R.P. Neves, M.T. Scotti, F.J.B. Mendonça-Junior, J. Braz. Chem. Soc. 32 (2021) 1017–1029.
[6] R.S. Cheke, V.M. Patil, S.D. Firke, J.P. Ambhore, I.A. Ansari, H.M. Patel, S. D. Shinde, V.R. Pasupuleti, M.I. Hassan, M. Adnan, A. Kadri, M. Snoussi, Pharmaceuticals 15 (2022) 272.
[7] M. Hassan, R. Ghaffari, S. Sardari, Y.F. Farahani, S. Mohebbi, Res. Pharm. Sci. 15 (2020) 281–290.
[8] A.S. Grewal, Int. J. Pharm. Res. 6 (2014) 1–7.
[9] H. Muğlu, M.S. Çavuş, T. Bakır, H. Yakan, J. Mol. Struct. 1196 (2019) 819–827.
[10] A. El-Faham, W.N. Hozzein, M.A.M. Wadaan, S.N. Khattab, H.A. Ghabbour, H.-K. Fun, M.R. Siddiqui, J. Chem. 2015 (2015) 1–8.
[11] H. Yakan, T.K. Bakır, M.S. Çavuş, H. Muğlu, Res. Chem. Intermed. 46 (2020) 5417–5440.
[12] G. Kiran, T. Maneshwar, Y. Rajeshwar, M. Sarangapani, J. Chem. 2013 (2013) 1–7.
[13] A. Singh, S. Ramsawroopand Kumar, Pharma Innovation 10 (2021) 643–646.
[14] H.B. Shawish, W.Y. Wong, Y.L. Wong, S.W. Loh, C.Y. Looi, P. Hassandarvish, A.Y. L. Phan, W.F. Wong, H. Wang, I.C. Paterson, C.K. Ea, M.R. Mustafa, M.J. Maah, PloS ONE 9 (2014) e100933.
[15] S.W. Ragsdale, J. Biol. Chem. 284 (2009) 18571–18575.
[16] M. Shabbir, Z. Akhter, A.R. Ashraf, H. Ismail, A. Habib, B. Mirza, J. Mol. Struct. 1149 (2017) 720–726.
[17] Ş. Güveli, B. Ülküseven, Polyhedron 30 (2011) 1385–1388.
[18] Y. Kaya, A. Erçağ, Ö. Uğuz, A. Koca, Y. Zorlu, M. Hacıoğlu, A.S. Birteksöz Tan, Polyhedron 207 (2021), 115372.
[19] M.M. Makhlouf, H.A. Alburaih, M.M. Shehata, M.S.S. Adam, M.M. Mostafa, A. El-Denglawey, J. Phys. Chem. Solids 151 (2021), 109817.
[20] M.M. Makhlouf, M.M. Shehata, Sol. Energy 211 (2020) 1128–1136.
[21] A.K. Singh, M.A. Quraishi, Mater. Chem. Phys. 123 (2010) 666–677.
[22] S.C.B. Oliveira, I.P.G. Fernandes, B.V. Silva, A.C. Pinto, A.M. Oliveira-Brett, J. Electroanal. Chem. 689 (2013) 207–215.
[23] B. Murukan, B. Sindhu Kumari, K. Mohanan, J. Coord. Chem. 60 (2007) 1607–1617.
[24] B. Murukan, K. Mohanan, Transition Met. Chem. 31 (2006) 441–446.
[25] B. Kaya, D. Akyüz, T. Karakurt, O. Şahin, A. Koca, B. Ülküseven, Appl. Organomet. Chem. 34 (2020) e5930.
[26] S. Duman, İ. Kızılcıklı, A. Koca, M. Akkurt, B. Ülküseven, Polyhedron 29 (2010) 2924–2932.
[27] Ş. Güveli, A. Koca, N. Özdemir, T. Bal-Demirci, B. Ülküseven, New J. Chem. 38 (2014) 5582–5589.
[28] B. Kaya, A. Koca, B. Ülküseven, J. Coord. Chem. 68 (2015) 586–598.
[29] Y. Kurt, A. Koca, M. Akkurt, B. Ülküseven, Inorg. Chim. Acta 388 (2012) 148–156.
[30] G.R. Burns, Inorg. Chem. 7 (1968) 277–283.
[31] Z. Juranić, F. Anastasova, I. Juranić, T. Stanojković, S. Radulović, N. Vuletić, J. Exp. Clin. Cancer Res. 18 (1999) 317–324.
[32] APEX2. version 2014.11-0, Bruker (2014), Bruker AXS Inc., Madison, WI.
[33] G.M. Sheldrick, Acta Crystallogr. Sect. A: Found. Adv. 71 (2015) 3–8.
[34] G.M. Sheldrick, Acta Crystallogr. Sect. C: Struct. Chem. 71 (2015) 3–8.
[35] O.V. Dolomanov, L.J. Bourhis, R.J. Gildea, J.A.K. Howard, H. Puschmann, J. Appl. Crystallogr. 42 (2009) 339–341.
[36] A.L. Spek, Acta Crystallogr. Sect. C: Struct. Chem. 71 (2015) 9–18.
[37] Y. Kaya, A. Erçağ, A. Koca, J. Mol. Struct. 1206 (2020), 127653.
[38] R. Apak, K. Güçlü, M. Özyürek, S.E. Karademir, J. Agric. Food Chem. 52 (2004) 7970–7981.
[39] W. Brand-Williams, M.-E. Cuvelier, C. Berset, LWT-Food Sci. Technol. 28 (1995) 25–30.
[40] A. Akbari, H. Ghateazadeh, R. Takjoo, B. Sadeghi-Nejad, M. Mehrvar, J.T. Mague, J. Mol. Struct. 1181 (2019) 287–294.
[41] S.A. Elsayed, H.E. Badr, A. di Biase, A.M. El-Hendawy, J. Inorg. Biochem. 223 (2021), 111549.
[42] S. Priyarega, P. Kalaivani, R. Prabhakaran, T. Hashimoto, A. Endo, K. Natarajan, J. Mol. Struct. 1002 (2011) 58–62.
[43] M.P. Sathisha, V.K. Revankar, K.S.R. Pai, Met.-Based Drugs (2008, 2008,) 1–11.
[44] H. Yakan, Ş. Çakmak, O. Buruk, A. Veyisoğlu, H. Muğlu, N. Türköz Karakullukçu, Res. Chem. Intermed. 48 (2022) 4331–4345.
[45] K. Gangarapu, S. Manda, A. Jallapally, S. Thota, S.S. Karki, J. Balzarini, E. De Clercq, H. Tokuda, Med. Chem. Res. 23 (2014) 1046–1056.
[46] M. Yıldız, M. Bingul, Y. Zorlu, M.F. Saglam, M. Boga, M. Temel, M.S. Koca, H. Kandemir, I.F. Sengul, Bioorg. Chem. 120 (2022), 105647.
[47] E. Ramachandran, P. Kalaivani, R. Prabhakaran, N.P. Rath, S. Brinda, P. Poornima, V.V. Padma, K. Natarajan, Metallomics 4 (2012) 218–227.
[48] P.X. García-Reynaldos, S. Hernández-Ortega, R.A. Toscano, J. Valdés-Martínez, Supramol. Chem. 19 (2007) 613–619.
[49] A.H. Kianfar, L. Keramat, M. Dostani, M. Shamsipur, M. Roushani, F. Nikpour, Spectrochim. Acta A Mol. Biomol. Spectrosc. 77 (2010) 424–429.
[50] B. Bouzerafa, A. Ourari, D. Aggoun, R. Ruiz-Rosas, Y. Ouennoughi, E. Morallon, Res. Chem. Intermed. 42 (2016) 4839–4858.
[51] L.-Q. Chai, H.-S. Zhang, J.-J. Huang, Y.-L. Zhang, Spectrochim. Acta A Mol. Biomol. Spectrosc. 137 (2015) 661–669.
[52] E. Canpolat, M. Kaya, J. Coord. Chem. 57 (2004) 1217–1223.

[53] M. Şahin, A. Koca, N. Özdemir, M. Dinçer, O. Büyükgüngör, T. Bal-Demirci, B. Ülküseven, Dalton Trans. 39 (2010) 10228–10237.
[54] K. Ohui, E. Afanasenko, F. Bacher, R.L.X. Ting, A. Zafar, N.r. Blanco-Cabra, E. Torrents, O. Dömötör, N.r.V. May, D. Darvasiova, E.v.A. Enyedy, A.R. Popović-Bijelić, Jóhannes, P. Rapta, M.V. Babak, G. Pastorin, V.B. Arion, J. Med. Chem. 62 (2018) 512-530.
[55] V.B. Arion, P. Rapta, J. Telser, S.S. Shova, M. Breza, K. Lušpai, J. Kozisek, Inorg. Chem. 50 (2011) 2918–2931.